Estimation of the Parameters of Continuous-time Systems using Data Compression

Liuping Wang[1] and Peter Gawthrop[2]

[1] Discipline of Electrical Energy and Control Systems, School of Electrical and Computer Engineering, RMIT University, Melbourne, Victoria 3000, Australia
liuping.wang@rmit.edu.au
[2] Centre for Systems and Control and Department of Mechanical Engineering, University of Glasgow, GLASGOW. G12 8QQ Scotland
P.Gawthrop@eng.gla.ac.uk

1 Introduction

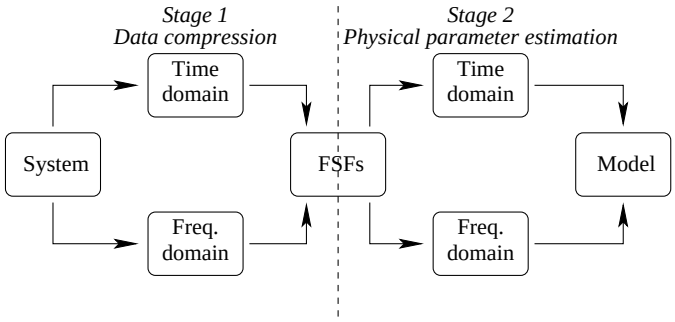

Fig. 1. Identification overview. Stage 1 identifies FSF parameters from either time or frequency data; stage two uses this compressed data to estimate either an empirical transfer function or the parameters of a physical model.

This chapter provides a unified introductory account of the estimation of the parameters of continuous-time systems using data compression based on a number of previous publications [23, 24, 26, 13, 25, 14].

The outline of the chapter is indicated in Figure 1. In particular, The core of our approach is the Frequency-sampling Filter (FSF) of Wang and Cluett[23, 24] where time or frequency domain data – within a predefined bandwidth – are represented as a set of (complex) filter coefficients; this can be viewed as a form of identification-orientated data compression.

The FSF coefficients are used to derive a system step response which is used in one of two ways:

1. to generate the parameters of a transfer function
2. to optimise the parameters of a physical model.

The methods will be described, analysed and also illustrated using data from a real example.

2 Frequency Sampling Filters

The book by Wang & Cluett[24] gives a comprehensive discussion of the frequency-sampled filter approach (including its relation to the discrete Fourier transform); this section provides a brief discussion of the material required for this paper. We consider linear time-invariant continuous-time systems with output $y(t)$ and input $u(t)$ uniformly sampled with time interval Δ to give input and output sequences $y_i = y(i\Delta)$ and $u_i = u(i\Delta)$. In the time-domain, the input and output sequences are related by $y_i = g_i * u_i$ where g_i is the discrete-time system impulse response and $*$ is the convolution operator. In the z-transform domain, $\bar{Y}(z) = \bar{G}(z)\bar{U}(z)$ where $\bar{Y}$ and $\bar{U}$ are the z-transforms of y_i and u_i respectively and $\bar{G}$ the corresponding transfer function. In this section, it is assumed that the system is *stable* and can be associated with an integer N; the number of time intervals after which the system impulse response is sufficiently small: $|g_i| < \epsilon \; \forall i > N$. The corresponding *settling-time* T is defined as:

$$T = N\Delta \tag{1}$$

The method can be extended to the unstable case[14].

The frequency-sampling filter FSF approach approximates the transfer function $\bar{G}(z)$ as:

$$\bar{G}_{fsf}(z) = \sum_{k=-\frac{n-1}{2}}^{\frac{n-1}{2}} \theta_k \bar{H}_k(z) \tag{2}$$

$$\bar{H}_k(z) = \frac{1}{N} \frac{1 - z^{-N}}{1 - \mathrm{e}^{j\Omega k} z^{-1}} \tag{3}$$

where n is odd, the *frequency sample interval* Ω is given by

$$\Omega = \frac{2\pi}{T} \tag{4}$$

$\bar{H}_k(z)$ is the kth *frequency sampling filter* (FSF) and θ_k the corresponding (complex) parameter. Alternatively, expressing frequency in Hz, define:

$$F = \frac{1}{T} = \frac{\Omega}{2\pi} \tag{5}$$

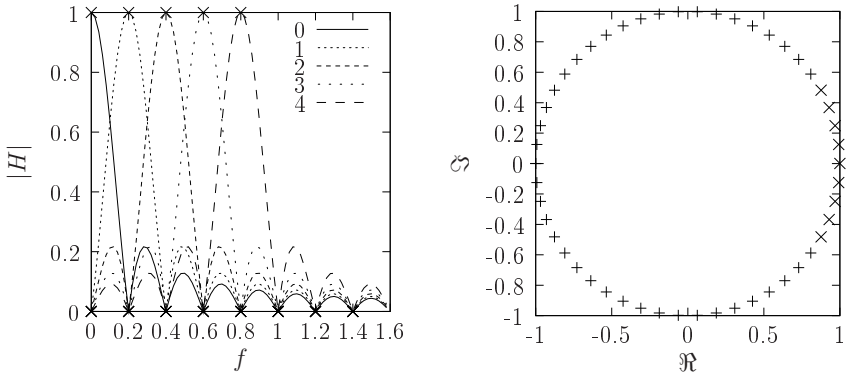

(a) Frequency responses (b) Pole locations

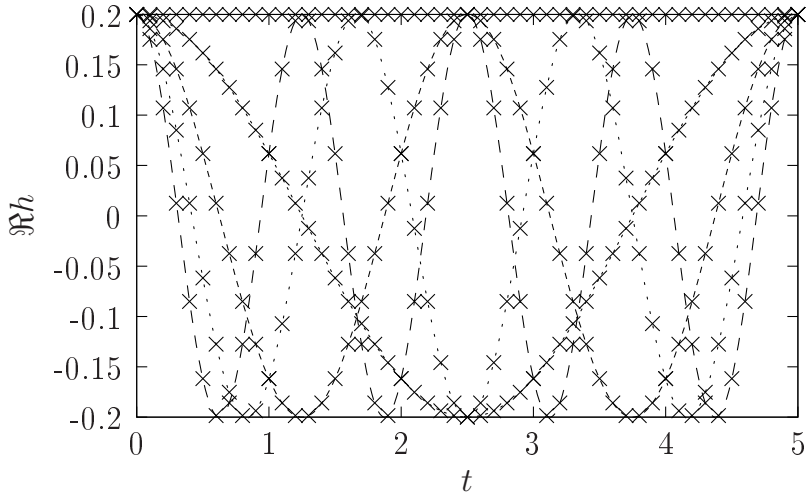

(c) Time responses

Fig. 2. Frequency-sampling filters: $n = 9$, $\frac{n-1}{2} = 4$, $T = 5$sec, $F = 0.2$Hz and $f_c = 0.8$

The name arises because the kth FSF has a frequency response with a peak at $\omega = k\Omega\text{rads}^{-1}$ or $f = kF\text{Hz}$.

Figure 2(a) shows the superimposed frequency responses of $|\bar{H}_k(z)|$ for $0 \leq k \leq 4$ when $T = 5$ (implying $F = 0.2$) for a frequency range $0 \leq \omega \leq 10$. The symbol "x" marks the frequency samples which coincide with the peaks of the FSFs. The kth filter of (3) has the discrete-time impulse response $\bar{h}_k(i)$

$$\bar{h}_k(i) = \frac{1}{N} \mathrm{e}^{j\Omega ki} \; i < N \tag{6}$$

As discussed by [23, 24], choosing $n = N$ gives an exact match $\bar{G}_{fsf}(z) = \bar{G}(z)$. Choosing $n < N$ gives an approximate match $\bar{G}_{fsf}(z) \approx \bar{G}(z)$ for a

frequency range $0 \leq \omega \leq N\Omega$. This situation is summarised in Figure 2(b) which shows $N = 50$ potential FSF poles (marked by "+") equispaced around the unit circle and the $n = 9$ actual FSF poles (marked by "x") clustered around $z = 1$ on the unit circle. It is natural to define a *cutoff frequency* f_cHz as the frequency of the peak of the highest frequency filter:

$$f_c = \frac{n-1}{2}F = \frac{n-1}{2T} \tag{7}$$

or the radian equivalent ω_c as:

$$\omega_c = 2\pi f_c \tag{8}$$

Particularly in the context of fast (with respect to system time constants) sampling, a good approximation can be obtained with $n << N$. The significance of this approximation lies in the fact that the neglected process frequency parameters correspond to higher frequency region of the system, which in many applications have severe noise corruption. In other words, f_c should be chosen to include the significant dynamics of the plant.

The FSF equation (2) can be rewritten in vector form as:

$$\bar{G}_{fsf}(z) = \theta^T \bar{F}(z) \tag{9}$$

where

$$\bar{F}(z) = \begin{pmatrix} \bar{H}_0(z) \\ \bar{H}_{-1}(z) \\ \bar{H}_1(z) \\ \cdots \\ \bar{H}_{-\frac{n-1}{2}}(z) \\ \bar{H}_{\frac{n-1}{2}}(z) \end{pmatrix} \qquad \theta = \begin{pmatrix} \theta_0 \\ \theta_{-1} \\ \theta_1 \\ \cdots \\ \theta_{-\frac{n-1}{2}} \\ \theta_{\frac{n-1}{2}} \end{pmatrix} \tag{10}$$

In time-domain terms:

$$y_i = \theta^T f_i * u_i \tag{11}$$

where f_i is the (discrete-time) impulse response corresponding to $\bar{F}(z)$. The convolution is, in practice performed by the usual time-domain filtering operation. Equation (9) is in the conventional linear-least squares form and so the parameter estimate $\hat{\theta}$ may be chosen to minimise a performance index of the form

$$J(M, \hat{\theta}) = \sum_{i=0}^{M} |e_i|^2 \tag{12}$$

where $e_i = y_i - \hat{y}_i$ and $\hat{y}_i$ is given by (11) with θ replaced by $\hat{\theta}$. Defining $Y_M = \begin{pmatrix} y_0 & y_1 & \ldots & y_M \end{pmatrix}^T$, $\phi_i = f_i * u_i$ and $\Phi_M = \begin{pmatrix} \phi_0 & \phi_1 & \ldots & \phi_M \end{pmatrix}^T$ then the Least Squares estimate is

$$\hat{\theta} = (\Phi_M^* \Phi_M)^{-1} \Phi_M^* Y_M \tag{13}$$

Although the FSF approach is cast in the discrete-time domain and the corresponding z-transform domain, the resultant model can be used to obtain continuous-time step and frequency responses as follows[24]. Using $z = \mathrm{e}^{\mathrm{i}\omega\Delta}$, (2) and (3) can be rewritten in frequency domain form as

$$G(\mathrm{i}\omega) \approx G_{fsf}(\mathrm{i}\omega) = \sum_{k=-\frac{n-1}{2}}^{\frac{n-1}{2}} \theta_k H_k(\mathrm{i}\omega) \tag{14}$$

$$H_k(\mathrm{i}\omega) = \bar{H}_k(\mathrm{e}^{\mathrm{i}\omega\Delta}) \text{ for } \omega < N\Omega \tag{15}$$

Similarly, the system impulse response $g(t)$ can be approximately computed using the continuous-time equivalent of (6)

$$g(t) \approx g_{fsf}(t) = \sum_{k=-\frac{n-1}{2}}^{\frac{n-1}{2}} \theta_k h_k(t) \tag{16}$$

$$h_k(t) = \frac{1}{T}\mathrm{e}^{jk\Omega t} \text{ for } t < N\Delta \tag{17}$$

And the step response $y_s(t)$ from:

$$y_s(t) = \int_0^t g(\tau)d\tau \tag{18}$$

In summary, the FSF method has *two* user-chosen parameters: the number of filters n (2) and the time-response settling time T (1). Using (4), (5), (7) and (8) these two parameters can be expressed as other pairs of parameters. One useful pair is:

Settling time T (1)
Cutoff frequency f_c (7)

3 Physical-model based estimation

Many engineering systems of interest to the control engineer are *partially known* in the sense that the system structure, together with some system parameters are known, but some system parameters are unknown. This gives rise to a problem of *parameter estimation* when values for the unknown parameters are to be determined from experimental data comprising measurements of system inputs and outputs. There is a considerable literature in the area including [1, 2, 3, 8, 7]. Although in special cases such identification may be *linear*-in-the parameters [1] or *polynomial*-in-the parameters [8, 7] in general the problem is *nonlinear*-in-the parameters. This means that, in general, the resultant optimisation problem is not quadratic or polynomial, and may even be non-convex. In such cases, the optimisation task is eased by knowing

(rather than deducing numerically) the first and second derivative of the error function with respect to the unknown system parameters.

Symbolic methods for nonlinear systems modelling, analysis and optimisation are currently strong research areas [20] driven by the ready availability of symbolic computational tools. In particular, the bond graph approach [16, 9, 11] has been used to generate models applicable to control design [6].

For the purposes of this paper, a *physically-plausible* model of a physical system is defined as a model that represents a different physical system that shares key behaviours of the actual system. Typically, the physically-plausible model will be simpler than the model itself and will be represented by a bond graph.

The advantages of having a simpler model are

- it is easier to understand a simple model than a complex model;
- the computation and numerical aspects of identification and control are eased.

The advantages of a physical model are that:

- the parameters of a physical model have a clearer interpretation than those of a purely empirical model and
- the behaviour of the model can be understood in physical terms.

The disadvantage of a physical model is that that it is *not* usually linear in the physical parameters thus leading to a non-linear optimisation problem. The *time-domain* parameter estimation problem posed in this paper is to estimate the unknown *physical* parameters Θ from the estimated system *impulse response* $g(t_i)$ at a finite number of discrete time instants $t_i, 1 \geq i \geq N_{opt}$. The usual least-squares estimation problem is posed; that is to minimise the cost function J with respect to the vector of unknown parameters Θ where:

$$J(\hat{\Theta}) = \frac{1}{2N_{opt}} \sum_{i=1}^{N_{opt}} e_i^2 \tag{19}$$

where the output error $e(t_i)$ is defined as

$$e_i = \hat{g}(t_i, \hat{\Theta}) - g(t_i, \Theta) \tag{20}$$

In a similar fashion the *frequency-domain* parameter estimation estimates Θ from the estimated *frequency response* $G(\mathrm{i}\omega_i)$ at a finite number of discrete frequencies $\omega_i, 1 \geq i \geq N_{opt}$ with:

$$e_i = \hat{G}(\mathrm{i}\omega_i, \hat{\Theta}) - G(\mathrm{i}\omega_i, \Theta) \tag{21}$$

These nonlinear least-squares problems does not admit an explicit solution in general; instead, numerical techniques must be used. Each iteration of such an algorithm requires evaluation of the function J for the current estimate $\hat{\Theta}$

and thus an evaluation of $\hat{g}(t_i, \hat{\Theta})$ or $\hat{G}(\mathrm{i}\omega_i, \hat{\Theta}$ for that value of $\hat{\Theta}$. Thus each iteration is computationally expensive and therefore an efficient algorithm is desirable.

A number of optimisation methods are available, the main division is between those that use gradient information and those that don't. The former have been discussed in this context previously [10, 12, 15] and include the Levenberg-Marquardt [5] and the "Projected BFGS-Armijo" algorithm of Kelley [17, Section 5.5.3]. The latter includes the Broyden-Fletcher-Goldfarb-Shanno (BFGS) method [5].

As the gradient based approaches have been considered preciously, this chapter uses the (non-gradient) BFGS method (as implemented as `bfgsmin` in Octave [4]).

4 Example: inverted pendulum

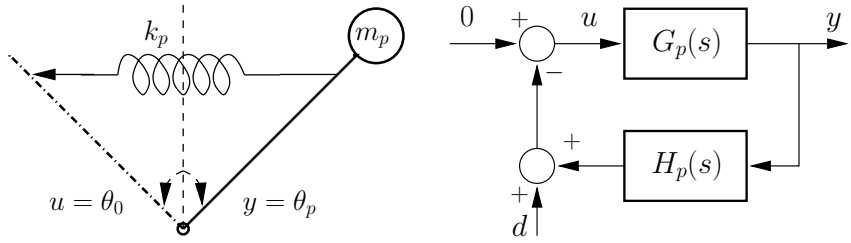

(a) Inverted Pendulum (b) Closed-loop system

Fig. 3. Experimental system

This section provides an illustrative example where the parameters of an inverted pendulum are identified using the two stage process of:

- identifying the FSF parameters from the closed-loop experimental data and
- identifying the physical parameters from the corresponding impulse or frequency responses.

A simple model human standing is equivalent to controlling an inverted pendulum (the body) via a spring (tendons and muscle) [19, Figure 1]. It is convenient to represent such a model by Figure 3(a) where the input u is the effective input angle θ_0 and the output y is the pendulum angle θ_p and the length of the pendulum is l. The system can be modelled with three parameters:

- the inertia about the pivot J_p
- the effective gravitational spring k_g and

- the ratio α of the effective spring constant to the gravitational spring.

Using the usual small angle approximation, the system has the transfer function:

$$G_p = \frac{\alpha k_g}{(1-\alpha)k_g - J_p s^2} \tag{22}$$

It is known [18] that $\alpha < 1$ (that is, the spring is not stiff enough to hold up the pendulum) so that the system of (22) is unstable and therefore requires regulation.

The feedback structure is given in Figure 3(b) where H_p is the stabilising controller and d a disturbance signal. The corresponding *closed-loop transfer function* $G(s)$ is given by

$$G(s) = \frac{y}{d} = -\frac{G_p(s)}{1 + G_p(s)H_p(s)} \tag{23}$$

As part of a programme to investigate the dynamics of human standing, an initial experimental setup replaces both pendulum and controller by digital equivalents within separate computers connected together, and to a third data-collection computer, via analogue instrumentation[3].

The data collected from this setup is used as an illustrative example in this chapter; it has the advantage the exact model is known. For the purposes of this chapter, a data set of length 100 seconds is used which has been sampled with interval $\Delta = 0.01$sec giving about 10000 data points for each signal. The input disturbance d is the multi-sine signal of Figure 4(a); it has the power spectral density shown in Figure 5.

To illustrate the properties of the FSF approach as noise levels increase, white noise with variance σ^2 is added to the measured output data y; the result is shown in Figures 4(b)-(d).

Figures 5(b)-(d) show some standard non-parametric estimation results for the data without any added noise. The empirical and Blackman-Tukey methods were computed using the "nonpar" function of the UNIT [21] toolbox.

4.1 FSF estimation

This section illustrates the use and behaviour of FSF using the data set d as input and data set y as output to identify the FSF parameters corresponding to the transfer function $G(s)$ (23). The results are displayed (Figures 6–8) in two forms, the modulus of the frequency response ($|G(\mathrm{i}\omega)$) and the corresponding impulse response $g(t)$; the figures are organised so that the frequency response is to the left and the time response to the right.

As discussed at the end of section 2, the FSF is parameterised by the cutoff frequency f_c and the settling time T.

[3] The data is used here was collected at the Department of Sports Science at the University of Birmingham in June 2006. It is used with the kind permission of Dr Martin Lakie and Dr Ian Loram.

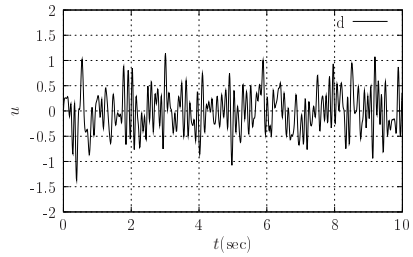

(a) Input disturbance d

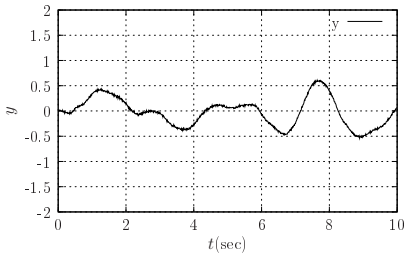

(b) Output y: $\sigma = 0.01$

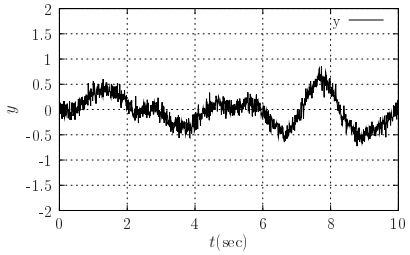

(c) Output y: $\sigma = 0.1$

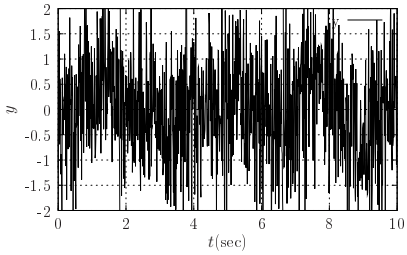

(d) Output y: $\sigma = 1$

Fig. 4. Data sampled with $\Delta = 0.01$sec. The first 10sec of 100sec of data is shown. Additional noise with standard deviation σ is artificially added to the system output to give Figures (b)–(d)

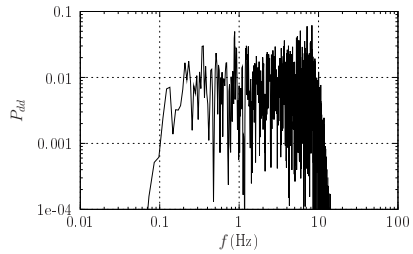

(a) Disturbance power spectral density

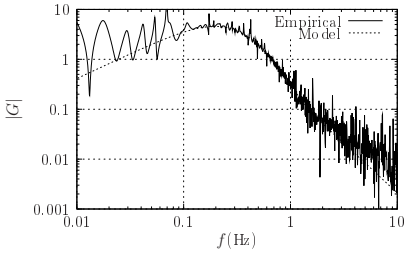

(b) Empirical frequency response

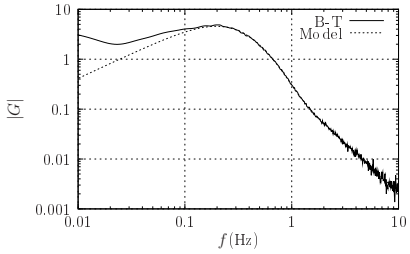

(c) Blackman-Tukey frequency response

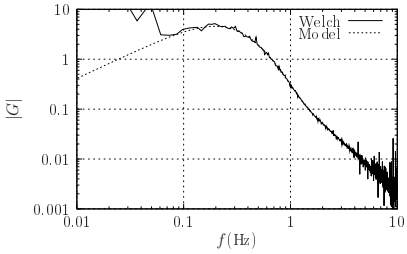

(d) Welch frequency response

Fig. 5. Other non-parametric methods

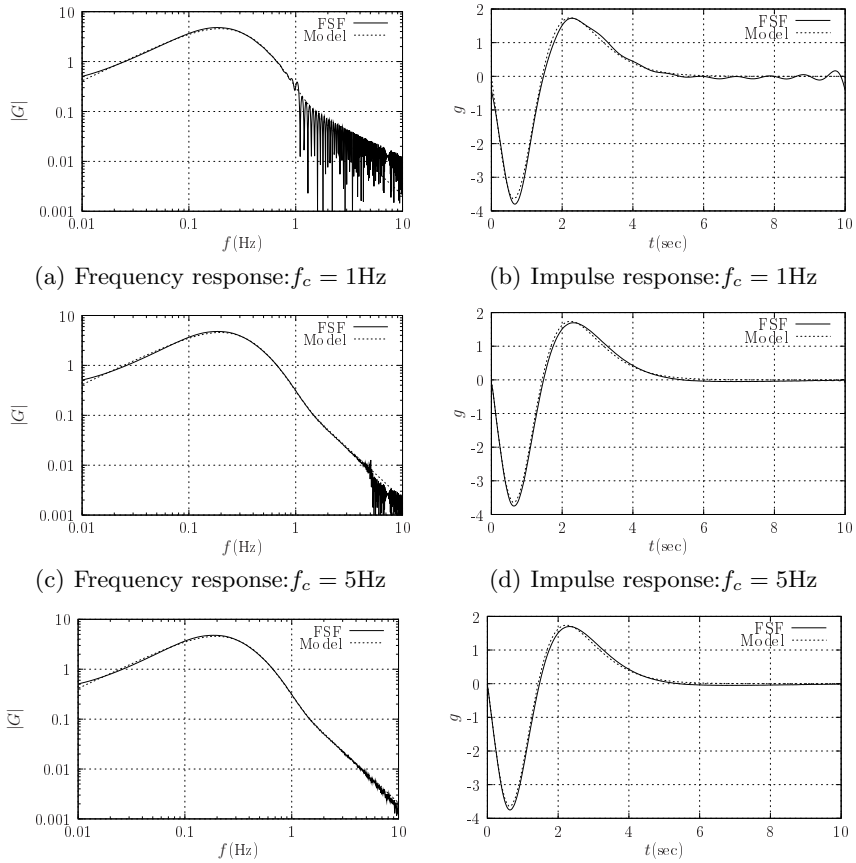

(a) Frequency response: $f_c = 1$Hz (b) Impulse response: $f_c = 1$Hz

(c) Frequency response: $f_c = 5$Hz (d) Impulse response: $f_c = 5$Hz

(e) Frequency response: $f_c = 10$Hz (f) Impulse response: $f_c = 10$Hz

Fig. 6. FSF properties: effect of cutoff frequency f_c ($T = 10$sec)

f_c is essentially a *frequency-domain* parameter and determines the largest *frequency* of interest. It also has time domain implications insofar as, from (7) it determines the number n of frequency-sampling filters used to approximate the impulse response given by (2). The effect of f_c is shown in Figure 6 for three values of f_c. Figures 6(a), 6(c) and 6(e) illustrate the fact that f_c determines the upper bound of the frequency for which the frequency response is matched by the FSFs.

T is essentially a time-domain parameter and determines the largest *time* of interest. It also has frequency domain implications insofar as, from (4), it fixes the *frequency-domain* sampling interval $\Omega = \frac{2\pi}{T}$. Figures 7(b), 7(d) and 7(f) illustrate the fact that T determines the upper bound of the time for which the time response is matched by the FSFs. These figures also

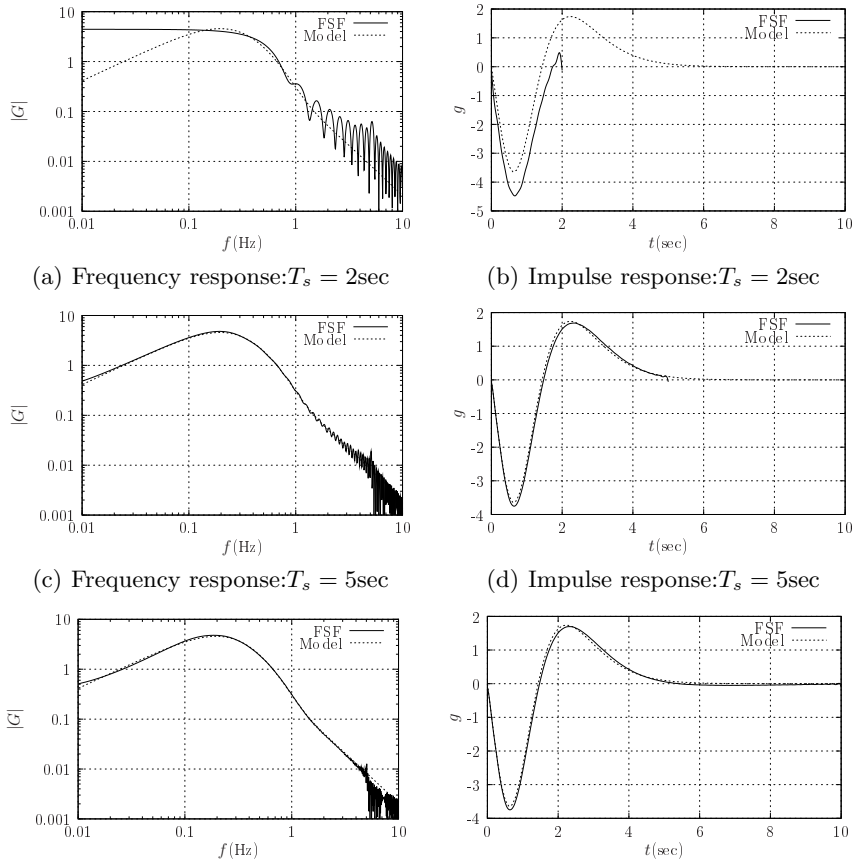

(a) Frequency response:$T_s = 2$sec (b) Impulse response:$T_s = 2$sec

(c) Frequency response:$T_s = 5$sec (d) Impulse response:$T_s = 5$sec

(e) Frequency response:$T_s = 10$sec (f) Impulse response:$T_s = 10$sec

Fig. 7. FSF properties: effect of settling time T_s ($f_c = 5$Hz)

show that if T is less than the actual settling time of the system, the estimated response is not accurate.

As with any identification technique, the FSF method is affected by measurement noise. The effect of measurement noise is illustrated by artificially adding noise to the data (Figures 4(b)–4(d)) to give Figure 8. As would be expected, the accuracy of both the time and frequency responses declines with increased measurement noise.

4.2 PMB estimation

As discussed in Section 3 the impulse and frequency responses estimated by the FSF can be transformed into a set of *physical* parameters Θ using a

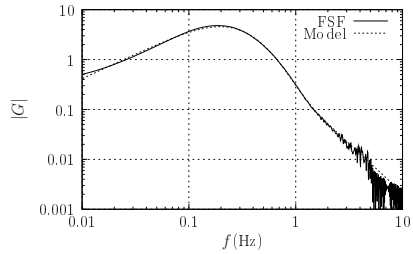

(a) Frequency response:$\sigma = 0.01$

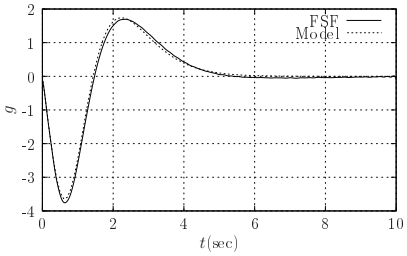

(b) Impulse response:$\sigma = 0.01$

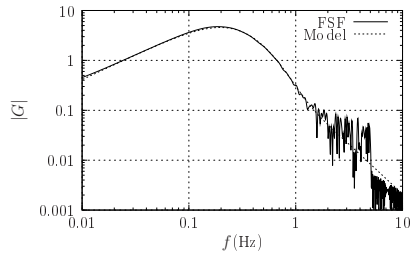

(c) Frequency response:$\sigma = 0.1$

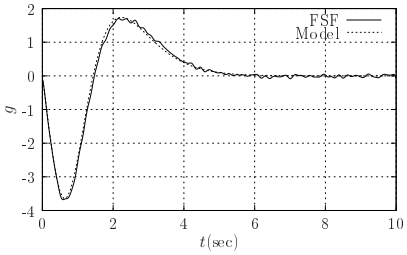

(d) Impulse response:$\sigma = 0.1$

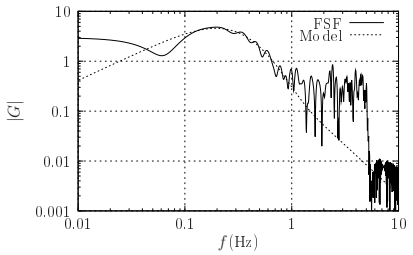

(e) Frequency response:$\sigma = 1$

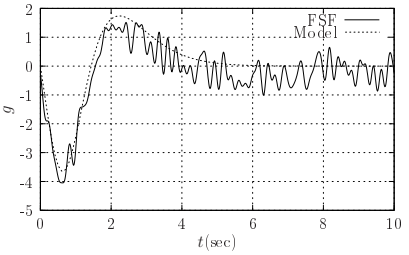

(f) Impulse response:$\sigma = 1$

Fig. 8. FSF properties: effect of noise level σ (($f_c = 5$Hz, $T_s = 10$sec))

Table 1. Estimated physical parameters (true values $\alpha = 0.85$, $J_p = 15$).

Domain	σ	$\hat{\alpha}$	$\hat{J}_p$
time	0.01	0.84	14.83
freq	0.01	0.84	15.05
time	0.10	0.84	14.78
freq	0.10	0.84	15.08
time	1.00	0.86	15.83
freq	1.00	0.87	16.71

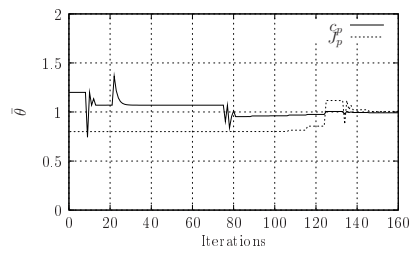

(a) Parameters: frequency domain

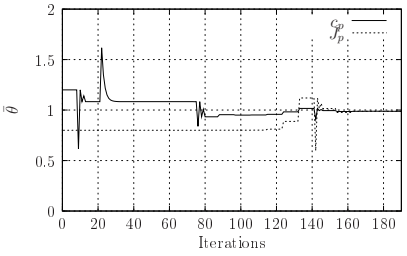

(b) Parameters: time domain

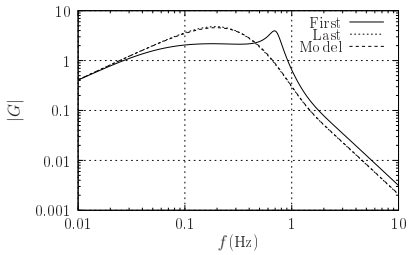

(c) Responses: frequency domain

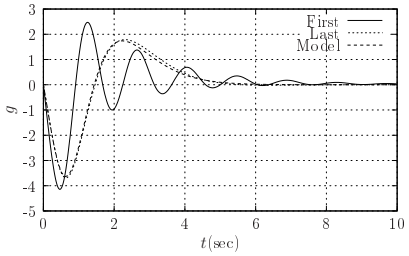

(d) Responses: time domain

Fig. 9. PMB estimation (low noise): $\sigma = 0.01$, $T = 10$sec and $f_c = 5$Hz

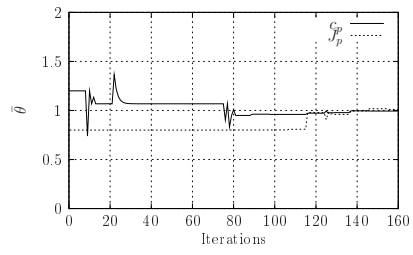

(a) Parameters: frequency domain

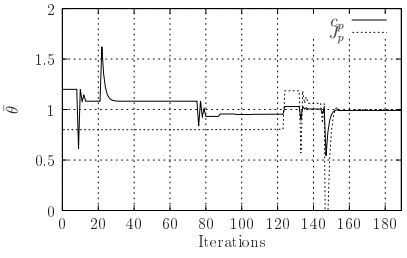

(b) Parameters: time domain

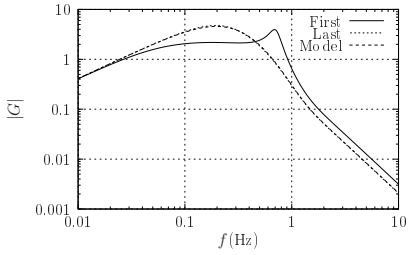

(c) Responses: frequency domain

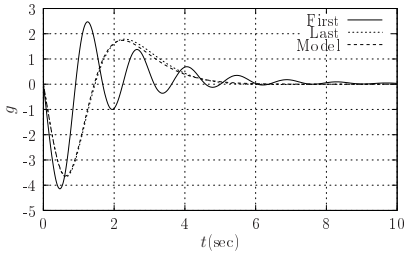

(d) Responses: time domain

Fig. 10. PMB estimation (medium noise): $\sigma = 0.1$, $T = 10$sec and $f_c = 5$Hz

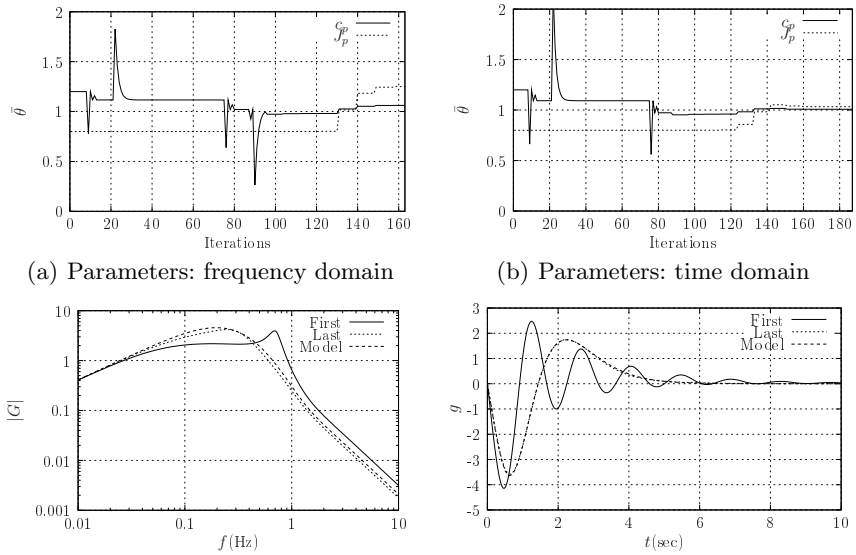

(a) Parameters: frequency domain

(b) Parameters: time domain

(c) Responses: frequency domain

(d) Responses: time domain

Fig. 11. PMB estimation (high noise): $\sigma = 1.0$, $T = 10$sec and $f_c = 5$Hz

non-linear optimisation approach such as that of Broyden-Fletcher-Goldfarb-Shanno (BFGS)[5] (here, the Octave [4] implementation `bfgsmin` is used). This is illustrated in this chapter by estimating two (α and J_p) of the three physical parameters (α, J_p k_g) of the experimental system of Figure 3 from each of the 6 FSF responses of Figure 8.

Figure 9 is based on the low-noise FSF responses of Figure 8(a)&(b). The left-hand figures correspond to frequency-domain optimisation (21) and the right hand figures to time-domain optimisation (20). The top row shows how the parameters evolve during the BFGS optimisation process; the bottom row shows responses corresponding to the first and last iterations together with the correct response for comparison.

Figure 10 is similar to 9 except that it is based on the medium noise responses of Figures 8(c)&(d).

Figure 11] is similar to 9 except that it is based on the high noise responses of Figures 8(e)&(f).

The resulting estimated parameters are shown in Table 1.

5 Conclusion

References

1. C. H. An, C. G. Atkeson, and J. M. Hollerbach. *Model-based Control of Robot Manipulators*. The MIT Press, 1988.
2. C. Canudas de Wit. *Adaptive control for partially known systems*. Elsevier, Amsterdam, 1988.
3. S. Dasgupta, B. D. O. Anderson, and R. J. Kaye. Output error identification methods for partially known systems. *Int. J. Control*, 43(1):177–191, 1986.
4. John W. Eaton. *GNU Octave Manual*. Network Theory Limited, 2002.
5. R. Fletcher. *Practical Methods of Optimization. 2nd Edition*. Wiley, Chichester, 1987.
6. P. J. Gawthrop. Physical model-based control: A bond graph approach. *Journal of the Franklin Institute*, 332B(3):285–305, 1995.
7. P. J. Gawthrop, J. Ježek, R. W. Jones, and I. Sroka. Grey-box model identification. *Control-Theory and Advanced Technology*, 9(1):139–157, 1993.
8. P. J. Gawthrop, R. W. Jones, and S. A. MacKenzie. Identification of partially-known systems. *Automatica*, 28(4):831–836, 1992.
9. P. J. Gawthrop and L. P. S. Smith. *Metamodelling: Bond Graphs and Dynamic Systems*. Prentice Hall, Hemel Hempstead, Herts, England., 1996.
10. Peter J Gawthrop. Sensitivity bond graphs. *Journal of the Franklin Institute*, 337(7):907–922, November 2000.
11. Peter J Gawthrop and Geraint P Bevan. Bond-graph modeling: A tutorial introduction for control engineers. *IEEE Control Systems Magazine*, 27(2), April 2007.
12. Peter J. Gawthrop and Eric Ronco. Estimation and control of mechatronic systems using sensitivity bond graphs. *Control Engineering Practice*, 8(11):1237–1248, November 2000.
13. P.J. Gawthrop and L. Wang. Transfer function and frequency response estimation using resonant filters. *Proceedings of the Institution of Mechanical Engineers Pt. I: Journal of Systems and Control Engineering*, 216(I6):441–453, 2002.
14. P.J. Gawthrop and L. Wang. Data compression for estimation of the physical parameters of stable and unstable linear systems. *Automatica*, 41(8):1313–1321, August 2005.
15. P.J. Gawthrop and L. Wang. Estimation of bounded physical parameters. In SYSID 2006 [22].
16. D. C. Karnopp, D. L. Margolis, and R. C. Rosenberg. *System Dynamics: A Unified Approach*. John Wiley, 1990.
17. C.T. Kelley. *Iterative Methods for Optimization*. Frontiers in Applied Mathematics. SIAM, Philadelphia, 1999.
18. Ian D. Loram and Martin Lakie. Direct measurement of human ankle stiffness during quiet standing: the intrinsic mechanical stiffness is insufficient for stability. *Journal of Physiology*, 545(3):1041–1053, 2002.
19. Ian D. Loram and Martin Lakie. Human balancing of an inverted pendulum: position control by small, ballistic-like, throw and catch movements. *Journal of Physiology*, 540(3):1111–1124, 2002.
20. Neil Munro, editor. *Symbolic methods in control systems analysis and design*. Number 56 in Control engineering series. IEE, Stevenage, UK, 1999.

21. B. Ninness and A. Wills. An identification toolbox for profiling novel techniques. In SYSID 2006 [22].
22. *14th IFAC (International Federation of Automatic Control) Symposium on System Identification, SYSID 2006*, Newcastle, New South Wales, Australia, March 2006.
23. L. Wang and W. R. Cluett. Frequency-sampling filters: an improved model structure for step-response identification. *Automatica*, Vol. 33(5):939–944, 1997.
24. L Wang and W R Cluett. *From Plant Data to Process Control*. Taylor and Francis, London and New York, 2000.
25. Liuping Wang, Peter Gawthrop, Charlie Chessari, Tony Podsiadly, and Angus Giles. Indirect approach to continuous time system identification of food extruder. *Journal of Process Control*, 14(6):603–615, September 2004.
26. Liuping Wang and Peter J Gawthrop. On the estimation of continuous time transfer functions. *Int. J. Control*, 74(9):889–904, June 2001.